

Arsenic trioxide inhibits human cancer cell growth and tumor development in mice by blocking Hedgehog/GLI pathway

Elspeth M. Beauchamp, ... , Jeffrey A. Toretsky, Aykut Üren

J Clin Invest. 2011;121(1):148-160. <https://doi.org/10.1172/JCI42874>.

Research Article

The Hedgehog (Hh) pathway is activated in some human cancers, including medulloblastoma. The glioma-associated oncogene homolog (GLI) transcription factors are critical mediators of the activated Hh pathway, and their expression may be elevated in some tumors independent of upstream Hh signaling. Thus, therapies targeting GLI transcription factors may benefit a wide spectrum of patients with mutations at different nodal points of the Hh pathway. In this study, we present evidence that arsenic trioxide (ATO) suppresses human cancer cell growth and tumor development in mice by inhibiting GLI1. Mechanistically, ATO directly bound to GLI1 protein, inhibited its transcriptional activity, and decreased expression of endogenous GLI target genes. Consistent with this, ATO inhibited the growth of human cancer cell lines that depended on upregulated GLI expression in vitro and in vivo in a xenograft model of Ewing sarcoma. Furthermore, ATO improved survival of a clinically relevant spontaneous mouse model of medulloblastoma with activated Hh pathway signaling. Our results establish ATO as a Hh pathway inhibitor acting at the level of GLI1 both in vitro and in vivo. These results warrant the clinical investigation of ATO for tumors with activated Hh/GLI signaling, in particular patients who develop resistance to current therapies targeting the Hh pathway upstream of GLI.

Find the latest version:

<https://jci.me/42874/pdf>





Arsenic trioxide inhibits human cancer cell growth and tumor development in mice by blocking Hedgehog/GLI pathway

Elspeth M. Beauchamp,¹ Lymor Ringer,¹ Gülay Bulut,¹ Kamal P. Sajwan,¹ Michael D. Hall,¹ Yi-Chien Lee,¹ Daniel Peaceman,¹ Metin Özdemirli,¹ Olga Rodriguez,¹ Tobey J. Macdonald,² Chris Albanese,¹ Jeffrey A. Toretsky,¹ and Aykut Üren¹

¹Lombardi Comprehensive Cancer Center, Georgetown University Medical Center, Washington, DC, USA.

²Department of Pediatrics, Emory University School of Medicine, Atlanta, Georgia, USA.

The Hedgehog (Hh) pathway is activated in some human cancers, including medulloblastoma. The glioma-associated oncogene homolog (GLI) transcription factors are critical mediators of the activated Hh pathway, and their expression may be elevated in some tumors independent of upstream Hh signaling. Thus, therapies targeting GLI transcription factors may benefit a wide spectrum of patients with mutations at different nodal points of the Hh pathway. In this study, we present evidence that arsenic trioxide (ATO) suppresses human cancer cell growth and tumor development in mice by inhibiting GLI1. Mechanistically, ATO directly bound to GLI1 protein, inhibited its transcriptional activity, and decreased expression of endogenous GLI target genes. Consistent with this, ATO inhibited the growth of human cancer cell lines that depended on upregulated GLI expression in vitro and in vivo in a xenograft model of Ewing sarcoma. Furthermore, ATO improved survival of a clinically relevant spontaneous mouse model of medulloblastoma with activated Hh pathway signaling. Our results establish ATO as a Hh pathway inhibitor acting at the level of GLI1 both in vitro and in vivo. These results warrant the clinical investigation of ATO for tumors with activated Hh/GLI signaling, in particular patients who develop resistance to current therapies targeting the Hh pathway upstream of GLI.

Introduction

While long recognized as critical in developmental biology, Hedgehog (Hh) signaling has rapidly become a pathway of intense study in oncology. The Hh pathway is activated in several cancers, such as basal cell carcinoma (BCC) and medulloblastoma (1–9). The pathway is composed of 3 Hh ligands (Sonic, Indian, and Desert Hh) that all bind to the Patched1 receptor. In the absence of Hh ligand, Patched inhibits the transmembrane protein Smoothed. When Patched is engaged by Hh, Smoothed is activated as a result of diminished inhibitory signal from Patched. The signal is then transduced to the downstream effectors GLI1, GLI2, and GLI3, which act as transcription factors.

While many Hh-driven human cancers involve either inactivation of Patched1 or activation of Smoothed, some tumors activate the pathway by increasing the protein levels of GLI independent of upstream Hh signaling. Examples of this alternative mechanism include *GLI* gene amplifications in rhabdomyosarcoma, osteosarcoma, glioma, and breast cancer (10–12); chromosomal translocations involving *GLI* in pericytoma (13); and increased GLI protein stability in prostate cancer (14). Additionally, we and others have previously shown that *GLI1* modulates Ewing sarcoma family of tumors (ESFT) carcinogenesis as a direct transcriptional target of Ewing sarcoma breakpoint region 1–Friend leukemia virus integration 1 (EWS-FLI1; refs. 15–17). Therefore, a novel therapy targeted to GLI would be beneficial for a wide spectrum of patients whose tumors have high GLI protein levels with an intact Patched/Smoothed axis.

Arsenic trioxide (ATO) is an FDA-approved drug used for the treatment of acute promyelocytic leukemia (APL) as a second line

of therapy for patients who do not respond or relapse on all-trans-retinoic acid therapy (ATRA). In APL, ATO's proposed mechanism of action is via degradation of the promyelocytic leukemia-retinoic acid receptor α (PML-RAR) fusion protein (18). Additional targets of ATO action in other tumor types include NF- κ B, thioredoxin reductase, and JNK (19–23). In the present study, we propose that one of ATO's mechanisms of action is through inhibiting the Hh/GLI pathway. Our data support the hypothesis that ATO could be clinically useful against tumors exhibiting activated Hh signaling, such as BCC, medulloblastoma, and ESFT.

Results

ATO inhibits GLI1 activity and reduces target gene expression. We investigated whether ATO inhibits GLI1 activity by measuring the GLI-responsive luciferase promoter pGL38xGLI, which contains 8 *GLI* DNA-binding sites attached to the chicken lens crystalline promoter followed by the luciferase gene. HepG2 cells, which do not express any detectable GLI1 protein or mRNA, were cotransfected with GLI1 and pGL38xGLI to examine the effect of ATO on GLI1 transcriptional activity. Cells were treated with vehicle or 0.1, 0.3, 1, 3, and 10 μ M of ATO for 24 hours. ATO was able to inhibit GLI1 transcriptional activity compared with vehicle control, with IC₅₀ of 2.7 μ M (Figure 1A). Cell viability was also evaluated in parallel to luciferase reporters at matching doses. We did not observe any reduction in cell viability at doses up to 10 μ M ATO and concluded that reduction in luciferase activity was not simply caused by cell death. To rule out the possibility that ATO nonspecifically inhibits transcription, translation, or luciferase activity, we then examined the effect of ATO on other transcription factors, including HES-1 (Notch) and EWS-FLI1 (Figure 1A and Supplemental Figure 1; supplemental material available online with this article; doi:10.1172/

Conflict of interest: The authors have declared that no conflict of interest exists.

Citation for this article: *J Clin Invest.* 2011;121(1):148–160. doi:10.1172/JCI42874.

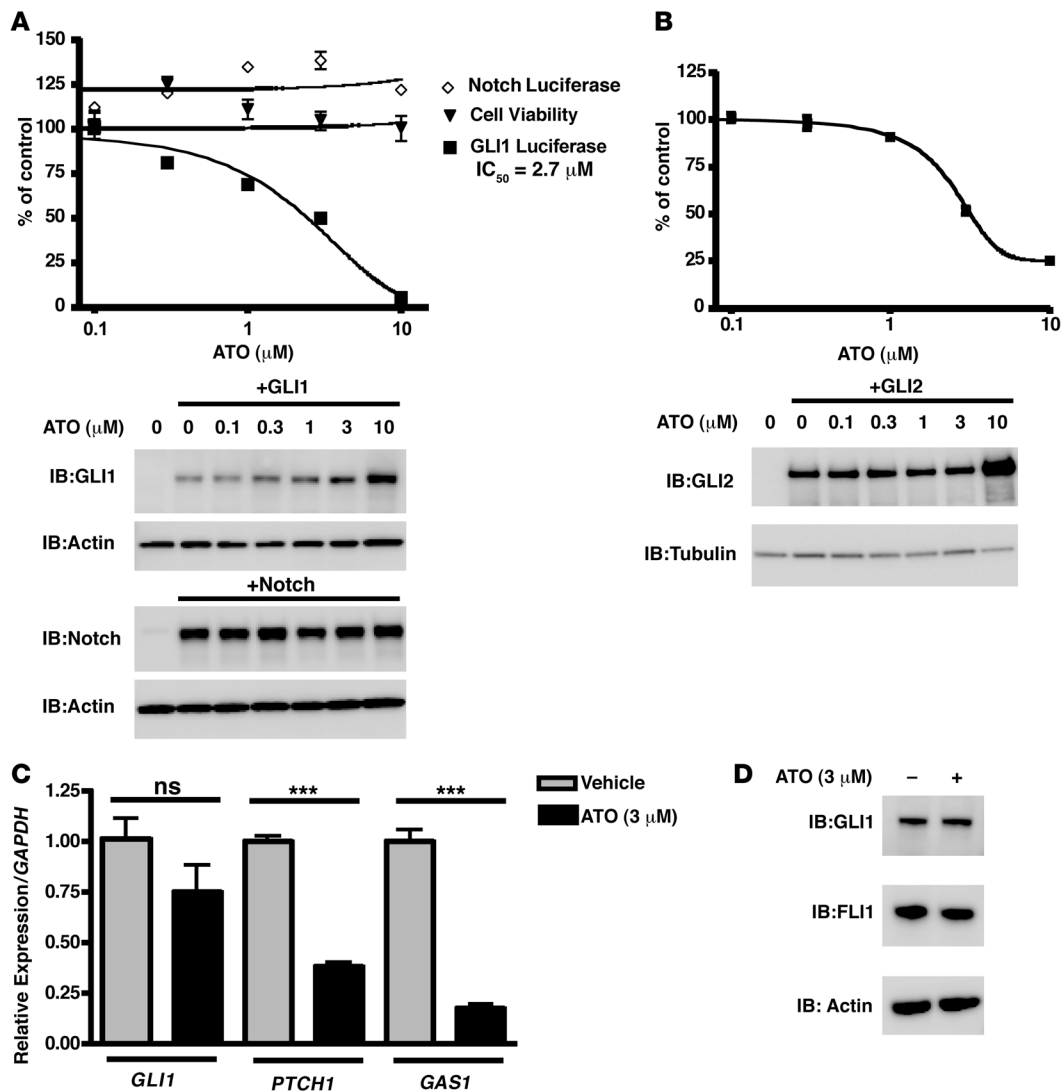


Figure 1

ATO inhibits GLI1 protein activity and target gene expression. (A and B) HepG2 cells were transfected with GLI1 luciferase reporter construct (pGL38XGLI) and Notch luciferase reporter construct (HES-1) with or without GLI1 and Notch cDNAs, respectively (A), and COS7 cells were transfected with pGL38XGLI and GLI2 constructs (B). *Renilla*-TK construct was used as transfection control for signal normalization. 24 hours after transfection, cells were treated with ATO for 24 hours. Mean \pm SD relative luciferase activity was calculated relative to *Renilla* activity. Transfection assays were performed in triplicate. Expression of GLI1 and Notch (A) and GLI2 (B) were detected by Western blot. In A, cell viability was measured at the same dose range and plotted on the same graph. (C) TC-71 cells were treated with vehicle or ATO for 12 hours. qRT-PCR was performed to quantify changes in *GLI1* mRNA levels as well as *PTCH1* and *GAS1*. Expression was normalized to *GAPDH*. Mean \pm SD relative expression level was calculated using the comparative Ct method. *** $P < 0.0001$, 2-tailed Student's *t* test. Each condition was performed in triplicate. (D) TC-71 total cell lysates from the experiment in C were subject to SDS-PAGE followed by IB with anti-GLI1, anti-FLI1, and anti-actin antibodies.

JCI42874DS1). ATO altered neither EWS-FLI1 nor Notch activity. Therefore, we concluded that ATO is able to specifically inhibit GLI1-modulated transcription. We also examined whether ATO inhibits GLI2 in addition to GLI1 by transfecting COS7 cells with GLI2 and the GLI-responsive luciferase construct. We observed inhibition of GLI2 activity by ATO similar to GLI1 (Figure 1B).

We also investigated whether ATO alters expression of endogenous GLI1 target genes, such as *PTCH1* and *GAS1*. The ESFT cell line TC-71 was treated with 3 μM ATO for 12 hours, and mRNA levels were measured for *GLI1*, *PTCH1*, and *GAS1* using quantitative RT-PCR

(qRT-PCR; Figure 1C). mRNA expression of *PTCH1* and *GAS1* was significantly reduced in cells treated with ATO. *GLI1* mRNA expression was only marginally inhibited by ATO, and the reduction was not statistically significant. Reduction in *GLI1* mRNA is likely caused by an inhibition of GLI1 activating its own promoter in an autoactivation loop (5). Although *GLI1* mRNA levels were reduced, there was no significant change of GLI1 protein expression at this time point, as assessed by IB (Figure 1D). Therefore, the decrease in target gene expression (*PTCH1* and *GAS1*) was not due to a decrease in GLI1 protein levels, but a decrease in GLI1 activity (Figure 1C).

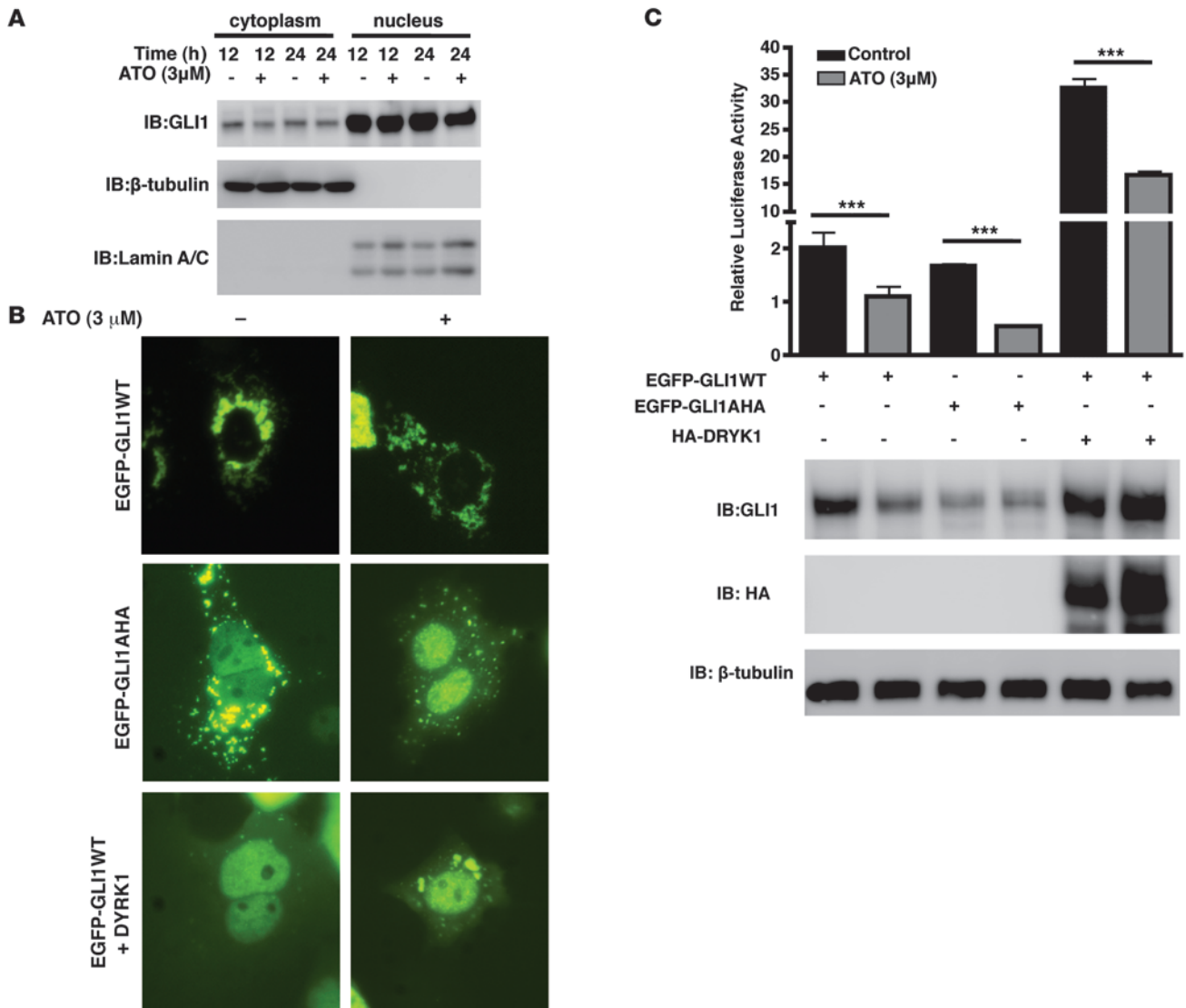
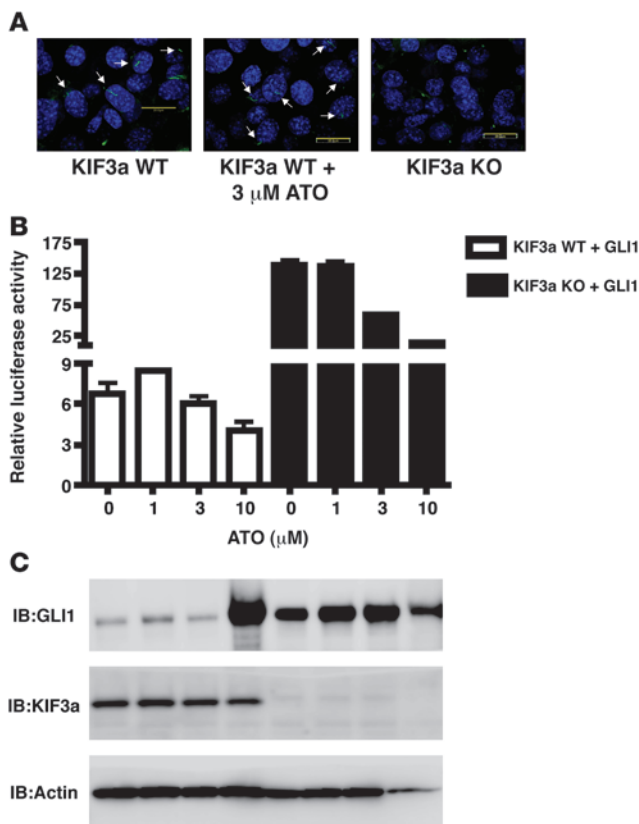


Figure 2

ATO does not change subcellular localization of GLI1. (A) TC-71 cells were treated with vehicle or ATO for 12 or 24 hours. Cell fractionation was conducted, and lysates were subject to SDS-PAGE followed by IB with the antibodies anti-GLI1, anti-β-tubulin (control for cytoplasmic proteins), and anti-lamin A/C (control for nuclear proteins). (B) Localization of EGFP-GLI1WT and EGFP-GLI1AHA; EGFP-GLI1WT with HA-DYRK1 was detected by green fluorescence. (C) COS7 cells were transfected with pGL38XGLI and EGFP-GLI1WT, EGFP-GLI1AHA, or EGFP-GLI1WT and HA-DRYK1. The Renilla-TK construct was used as a control for normalization. 24 hours later, cells were treated for 24 hours with 3 µM ATO. Mean ± SD relative luciferase activity was calculated relative to Renilla activity. ***P < 0.0001, 2-tailed Student's t test. Transfection assays were performed in triplicate. Expression of GLI constructs were detected by Western blot.

ATO does not alter intracellular localization of GLI1. ATO has been previously shown to cause degradation of the fusion protein PML-RAR in APL cells (18). However, we did not observe degradation of GLI1 protein in response to ATO treatment (Figure 1). We therefore investigated whether ATO affects intracellular trafficking of GLI1. To follow endogenous GLI1, we performed cell fractionation in the ESFT cell line TC-71 after cells were treated with 3 µM ATO for 12 and 24 hours (Figure 2A). We examined whether there were any changes in GLI1 protein levels in the cytoplasm compared with the nucleus. Total GLI1 protein levels did not change, nor were shifts observed between the nuclear and cytoplasmic pools. These data indicate that the effect of ATO on GLI1 activity does not occur by

altering its subcellular localization. We corroborated these observations by using fluorescence microscopy to assess the localization of GFP-tagged GLI1 in COS7 cells. Overexpression of GLI1 protein in cells with low Hh activity resulted in accumulation of GLI1 in the cytoplasm. Compared with the abundant amount of protein in the cytoplasm, the small amount of GFP-tagged GLI1 transported into the nucleus, which activates transcription in reporter assays, is usually too faint to detect by fluorescence microscopy. Two different approaches helped overcome this technical challenge. The mutation of the nuclear export signal sequence in GLI1, or the presence of Dryk1 kinase to phosphorylate GLI1, results in activated Hh pathway by maintaining nuclear localization of GLI1 protein

**Figure 3**

ATO does not inhibit GLI1 by affecting primary cilia. **(A)** Effects of ATO on primary cilia were visualized using confocal fluorescence microscopy on MEFs stained for acetylated tubulin. Arrows indicate cilium. Scale bars: 20 μ m. **(B)** KIF3a WT and knockout cells were transfected with pGL38XGLI and EGFP-GLI1. The *Renilla*-TK construct was used as a control for normalization. 24 hours later, cells were treated for 24 hours with ATO at 1, 3, and 10 μ M. Mean \pm SD relative luciferase activity was calculated relative to *Renilla* activity. Transfection assays were performed in triplicate. **(C)** Expression of GLI1 and KIF3a were detected by IB.

the cells to form cilia. Cells were then treated with 3 μ M ATO for 24 hours and fixed and stained by immunofluorescence for acetylated tubulin to visualize cilia (Figure 3A). ATO had no effect on cilia formation, as shown by confocal microscopy. The knockout MEFs were used as a negative control and, as expected, did not form cilia. We then looked at the effect of ATO on GLI1 activity as measured by the GLI-responsive luciferase construct in the KIF3a WT and knockout MEFs. Previous studies established that in cases of upstream pathway activation, such as active Smoothened, primary cilia are required for tumorigenesis. Conversely, if a tumor is activated at the level of GLI, the presence of primary cilia is inhibitory (32, 33). The KIF3a knockout MEFs showed higher GLI1 activity following transfection with GLI1 (Figure 3B), consistent with previously published observations (32, 33). ATO was able to inhibit GLI1 in the WT and knockout MEFs. These results indicate that ATO inhibits GLI1 function independent of the primary cilia.

ATO directly interacts with GLI1 protein, but does not inhibit GLI1 binding to DNA. In order to test whether ATO binds directly to GLI1, we took 2 different approaches. First, we expressed and partially purified recombinant human GLI1 protein with a 6xHis tag to perform in vitro binding assays (Figure 4A). Full-length recombinant GLI1 has been elusive and not described in the literature as a result of its large size, poor solubility, and high level of disorder. We produced recombinant GLI1 through a refolding protocol that worked for a different disordered protein, EWS-FLI1 (34). This partially purified GLI1 was enriched sufficiently for direct ATO binding studies and DNA binding studies with surface plasmon resonance (SPR). To determine whether ATO directly binds to GLI1, we used a method that was previously used to assess binding of arsenite to IKK β (21). We performed competitive binding assays between ATO and 4',5'-bis(1,3,2-dithioarsolan-2-yl)fluorescein-(1,2-ethanedithiol)2 (FLAsH-EDT₂), a green fluorescent organoarsenical that gives enhanced signal when bound to a protein (35). In the presence of GLI1, there was an approximately 2-fold increase in the fluorescence signal over the control (Figure 4B), which indicates that FLAsH is able to bind to GLI1. FLAsH compound did not bind to recombinant EWS-FLI1, which was used as a negative control to rule out nonspecific interaction. Increasing amounts of ATO competed with FLAsH binding to recombinant GLI1, which indicates that ATO is binding directly to GLI1. This decrease was statistically significant at 200 μ M. Excess 2,3-dimercaptopropanol (BAL) is able to quench the signal of FLAsH and was used as a positive control in the competitive binding studies.

In the second approach, we expressed EGFP-GLI1 in COS7 cells, treated cells with 2.5 μ M 4,5-bis(1,2,3-dithiarsolan-2-yl)resorufin-(1,2-ethanedithiol)2 (ReAsH-EDT₂), and assessed their colocalization by confocal fluorescence microscopy. We used EGFP alone and EGFP-Dishevelled-3 (EGFP-DVL3) as negative controls. ReAsH-EDT₂ did not bind to either EGFP or EGFP-DVL3 proteins,

(24). COS7 cells were transfected with expression vectors for either WT GLI1 (EGFP-GLI1WT), GLI1 that has the end of its nuclear export signal mutated from LRLD to AHAD (EGFP-GLI1AHA), or WT GLI1 cotransfected with DYRK1 (Figure 2B and Supplemental Figure 2). Cells were treated with 3 μ M ATO for 24 hours. There was no change in localization of the WT GLI1, which remained mainly cytoplasmic. In addition, ATO did not alter the nuclear localization of EGFP-GLI1AHA or of GLI1 cotransfected with DYRK1. We also tested whether ATO inhibits GLI1 transcriptional activity if GLI1 protein is restricted to the nucleus (Figure 2C). Treatment with 3 μ M ATO for 24 hours inhibited WT GLI1-, GLI1AHA mutant-, and DYRK1-mediated transcriptional activation of GLI1. These results suggest that ATO is able to inhibit GLI1 in the nucleus. These findings do not rule out any effect ATO may still have in the cytoplasm, and the observed phenotype may be a combination of ATO's effect on different pathways in both cytoplasm and nucleus. However, the data presented in Figure 2 strongly argue that ATO can inhibit GLI1 function in the nucleus without altering its protein stability in the cytoplasm.

ATO's inhibition of GLI1 does not require primary cilia. Recent evidence has shown that primary cilia play an important role for Hh pathway signal transduction (25–31). This cilia-Hh connection was first discovered when mice carrying mutations for intraflagellar transport proteins required for cilia formation showed developmental defects similar to that seen in Hh signaling mutants (27, 28). Therefore, we examined whether ATO has an effect on primary cilia and thereby inhibits GLI function. We used mouse embryonal fibroblasts (MEFs) that were WT or had homozygous deletion of the intraflagellar transport protein KIF3a. WT and knockout MEFs were grown to confluency and then serum starved to force

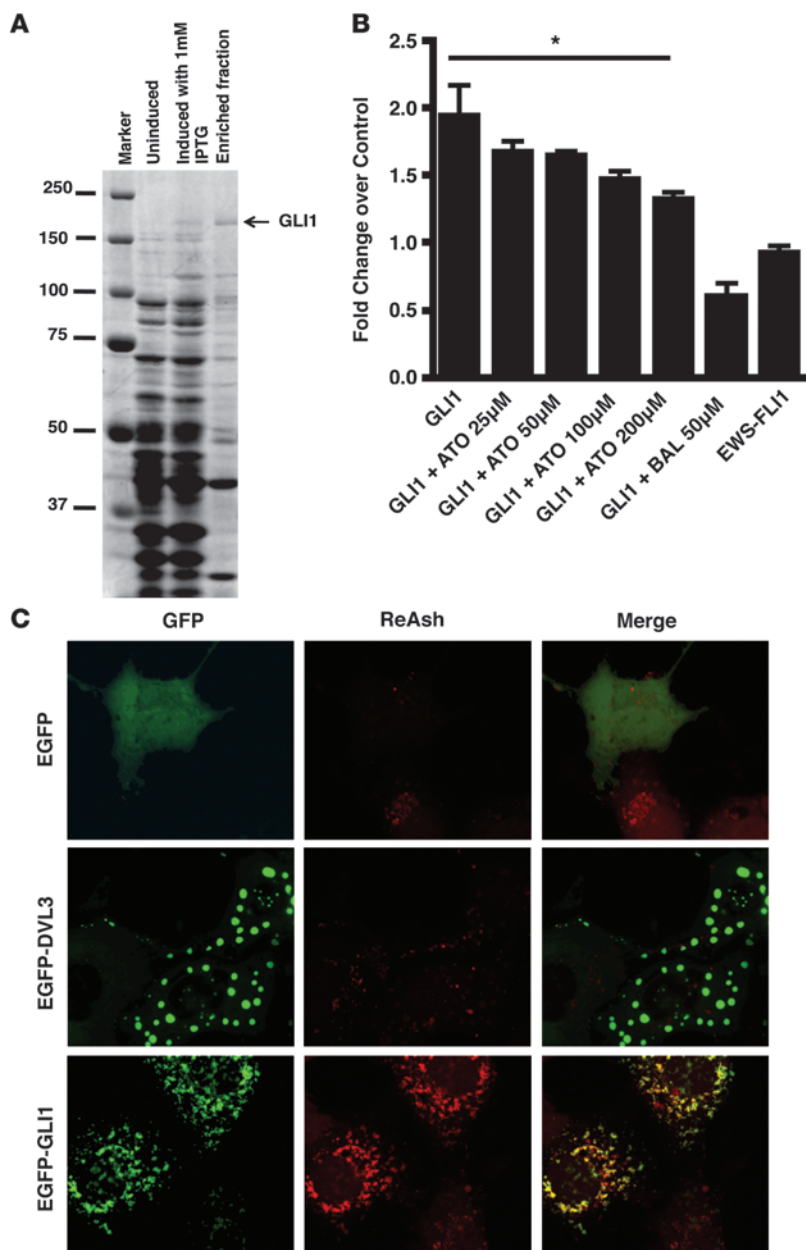


Figure 4

ATO directly binds to GLI1. (A) Coomassie-stained gel shows induction of full-length GLI1 protein expression in bacteria. Protein in the inclusion bodies was bound to Ni⁺ NTA column, refolded on the column, and eluted with an imidazole gradient. IPTG, isopropyl-D-1-thiogalactopyranoside. (B) 40 nM full-length GLI1 protein was preincubated with either BAL (50 µM for 10 minutes) or ATO (200, 100, 50, and 25 µM for 2 hours). 200 nM FIAsh-EDT was then added for 20 minutes. EWS-FLI1 with 200 nM FIAsh was used as negative control. Fluorescence intensity was measured with excitation at 508 nm and emission at 528 nm; relative fluorescence intensity is expressed as the fold change over the control (FIAsh alone). **P* = 0.02, 2-tailed Student's *t* test. (C) COS7 cells were transfected with EGFP alone, EGFP-DVL3, and EGFP-GLI1 and then treated with 2.5 µM ReAsH-EDT₂ for 1 hour. Colocalization was examined by confocal fluorescence microscopy (all images are at x600 magnification).

but bound to GLI1 and gave a yellow emission through confocal microscopy (Figure 4C). We also attempted to directly measure direct binding affinity of ATO to GLI1 in SPR studies. However, because of the very high ratio of molecular weights of ATO to recombinant GLI1 protein and the limited amount of GLI1 protein that can be captured on a Biacore chip, we could not measure direct ATO binding by SPR.

We next sought to define the mechanism of ATO inhibition of GLI1 by evaluating ATO's effects on DNA binding. We immobilized GLI1 protein to a CM5 chip in a Biacore T-100 instrument (Supplemental Figure 3A). DNA binding kinetics were measured by injecting double-stranded oligonucleotides that contain a consensus *GLI* DNA binding sequence from the *PTCH1* promoter (36). As a negative control, we used the same 19-bp oligonucleotide in which the consensus sequence was mutated. GLI1 bound

to its putative WT DNA consensus site with 8.15 nM *K_d*, but did not bind to the mutated sequence. Coinjection of 10 µM ATO did not inhibit binding of WT oligonucleotide to GLI1. A reciprocal experiment, in which biotinylated oligonucleotides were immobilized onto a streptavidin surface as the ligand and GLI1 injected as the analyte, demonstrated similar results (data not shown).

ATO is cytotoxic toward cells with active Smoothed/Gli pathway. Our prior investigations, along with publications by other groups, have established GLI1 as an important transcription factor for ESFT tumorigenesis (15–17). GLI activation as a downstream target of the Hh pathway has been actively studied in tumors with constitutively activated Smoothed (caused by *PTCH1* mutation or loss), such as BCC and medulloblastoma. Since ATO is able to inhibit GLI1 transcriptional activity, we hypothesized that ATO is cytotoxic in cell lines dependent on GLI, such as Ewing sarcoma (ES)



Table 1
IC₅₀ values for cell lines treated with ATO

Cell line	Histology	IC ₅₀ at 4 days (μM)
TC-71	ESFT	0.6
RDES	ESFT	0.9
ES925	ESFT	0.9
A4573	ESFT	0.5
CHP-100	ESFT	0.8
SKES	ESFT	0.3
TC-32	ESFT	1.4
A673	ESFT	0.5
MMH ES-1	ESFT	0.5
STA.ET.7.2	ESFT	0.9
DAOY	Medulloblastoma	0.4
D556	Medulloblastoma	0.4
HepG2	Hepatocellular carcinoma	6.6
PANC1	Pancreatic adenocarcinoma	9.1
CAPAN1	Pancreatic adenocarcinoma	9.0
H1299	Non-small-cell lung cancer	2.9
HEK293	HEK	2.3

Cells were plated in a 96-well plate and treated with vehicle or ATO at doses 1 nM to 10 μM. IC₅₀ values were calculated using a nonlinear sigmoidal dose-response curve fit.

and medulloblastoma. We treated various cancer cell lines with either vehicle or a dosage range from 1 nM to 10 μM of ATO for 4 days and determined IC₅₀ values (Table 1 and Supplemental Figures 4 and 5). HepG2, PANC1, CAPAN1, H1299, and HEK293 were used as negative control cell lines, as they expressed low or no detectable levels of GLI1 by Western blot (Figure 5A). The average IC₅₀ for ESFT and medulloblastoma cell lines was 0.68 μM, a 9-fold difference compared with 5.98 μM for the control cell lines ($P < 0.0001$, 2-tailed Student's *t* test), which lends further support to the notion that cells dependent on active GLI signaling may be more sensitive to ATO treatment.

ESFT cell lines, such as TC-71, SKES, and A4573, that expressed the highest levels of GLI1 and/or GLI2 were also the most sensitive to ATO. TC-32 was the least sensitive ESFT cell line and also had the least GLI1 and GLI2 protein expression (Figure 5A). Sensitivity to ATO correlated with GLI protein levels: the relative total GLI levels, as measured by densitometry of the IB (Figure 5A), plotted versus the IC₅₀ values (Table 1), showed a statistically significant correlation (Figure 5B). Furthermore, modulation of GLI1 protein levels in COS7 cells altered their response to ATO treatment. Transient transfection of GLI1 to COS7 cells induced enhanced proliferation, which was inhibited by 1 μM ATO (Supplemental Figure 6A). Reducing GLI1 protein expression by siRNA in COS7 cells resulted in resistance to ATO (Supplemental Figure 6B).

We investigated the possibility that ATO's cytotoxic effects are caused, at least in part, by JNK or NF-κB. We treated TC-71 cells with 3 μM ATO and 10 μM of the JNK inhibitor SP600125 for 24 hours (Supplemental Figure 7A). As previously published, ATO activated JNK in TC-71 cells, as measured by Western blot for phospho-JNK. However, when JNK was inhibited, ATO was still able to kill TC-71 cells. Moreover, JNK inhibition had no effect on the ability of ATO to inhibit GLI1 activity (Supplemental Figure 7B). This rules out the possibility that ATO's effects are caused by JNK. We also treated cells with 3 μM ATO alone or in combination with the NF-κB activator LPS at 10 μg/ml for 24 hours (Supplemental

Figure 8). In this case, we did not see inhibition of NF-κB by ATO, as measured by Western blotting for phospho-NF-κB p65. Moreover, activation of NF-κB had no effect on ATO's ability to kill TC-71 cells. These data rule out the possibility that ATO's effects are caused by NF-κB.

ATO inhibits in vivo growth of ESFT. We established ESFT xenografts by orthotopically injecting TC-71 cells into the gastrocnemius of SCID mice. Tumor growth was monitored daily with caliper measurements. Animals with palpable tumor masses were randomly assigned to either control or treatment groups. Injections of 0.15 mg/kg ATO or PBS vehicle were given i.p. every other day, and tumor volume measurements were continued daily. In most previous animal studies, a dose of 2.5–10 mg/kg of ATO was used (37–40). However, these studies used a compound purchased from Sigma-Aldrich, which was not pharmaceutical grade. We compared the potency of the pharmaceutical grade ATO (Cephalon) with that of the Sigma-Aldrich compound at 10 and 30 μM by treating COS7 cells for 24 hours (Supplemental Figure 9). At both doses, the Cephalon compound was significantly more cytotoxic than the Sigma-Aldrich compound. Therefore, we decided to use the dose of 0.15 mg/kg used in human patients. Animals were euthanized when their tumor volume reached 1 cm³. The tumor growth rate of TC-71 xenografts was extremely rapid. Mice developed palpable tumors within 2–4 weeks after implantation, and control mice had to be euthanized 7 days after the start of treatment. Despite the rapid growth rate of tumors, a statistically significant decrease in tumor growth was measured in mice treated with ATO (Figure 6A). Tumors from mice treated with ATO were compared with those receiving vehicle treatment by histology and immunohistochemistry (IHC) for TUNEL staining as a measure of apoptosis. The tumors of mice treated with ATO showed marked gross necrosis compared with control mice at the initial dissection (Figure 6B). Liquefied necrotic tissue was not a part of the formalin-fixed sections. The tissue that could be analyzed by H&E also showed large areas of necrosis in ATO-treated tumors. In areas of non-necrotic tissue, the ATO-treated tumors showed a trend toward increased apoptosis by TUNEL staining compared with the control tumors; however, this was not statistically significant. There was no significant difference in the morphology of the tumors in viable tumor areas or in the number of mitoses per slide between control and ATO-treated animals.

A new set of animals was orthotopically injected with TC-71 cells and observed until they formed palpable tumors. They were then treated with ATO and euthanized at 3 and 24 hours after i.p. injection, before the tumors became necrotic. We performed qRT-PCR for GLI target genes *PTCH1* and *GAS1* in frozen tissue from control and ATO-treated mice (Figure 6C). We observed a decrease in GLI target gene expression of *PTCH1* and *GAS1* after ATO treatment in vivo, which was statistically significant at both 3 and 24 hours for *PTCH1* and at 24 hours for *GAS1*. This finding suggested that tumors were exposed to an effective dose of ATO in vivo.

We also examined whether GLI1 was being degraded in vivo in tumors. Similar to in vitro studies with ESFT cell lines, there was no difference in GLI1 protein levels between control and ATO-treated animals (Figure 6D).

ATO increases survival of constitutively activated Smoothed transgenic mice with medulloblastoma. The ND2:SmA1 transgenic model contains an activated Smoothed receptor in which codon 535 is changed from Trp to Leu. The transgene is under the control of the ND-2 promoter, which provides selective expression in gran-

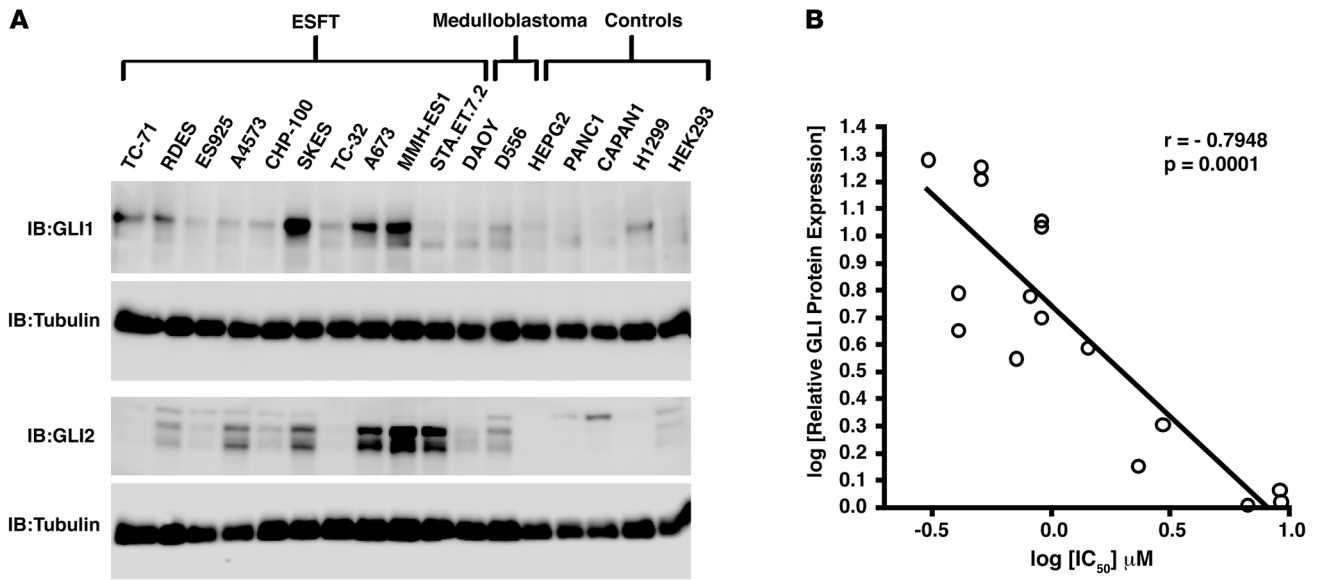


Figure 5 ATO sensitivity correlates with GLI expression. (A) Whole cell lysates were subject to SDS-PAGE followed by IB with anti-GLI1, anti-GLI2, and anti-β-tubulin antibodies. (B) log relative GLI expression, as measured by densitometry of Western blots in A, versus log IC₅₀ from Table 1. Correlation was assessed using nonparametric Spearman test ($r = -0.7948$, $P = 0.0001$).

ule neuron precursor cells of the cerebellum and results in a high incidence of medulloblastoma (41, 42). In our study, we used mice that were homozygous for the transgene. Approximately 50% of the animals showed medulloblastomas, and tumor growth was less aggressive compared with previously published results. Only animals with tumors were included in this study. Tumors were detected by MRI (Figure 7A) and monitoring for the presence of clinical signs of disease, such as decreased motor and coordination functions, deformed cranium, megalencephaly, hunched back, and weight loss. Once a tumor was detected, animals were treated with ATO at a dose of 0.15 mg/kg 3 times per week. The survival of these mice was compared with that of untreated mice (Figure 7B). ATO treatment increased survival significantly ($P = 0.0015$, Kaplan-Meier analysis). All animals received at least 1 diagnostic MRI around 4 months of age. Average age at the initial MRI was 4.4 ± 0.4 months for control and 4.6 ± 0.6 months for ATO ($P = 0.6919$, 2-tailed Student's t test). Average tumor size at that time was 185.2 ± 45.4 mm³ for control and 152.2 ± 53.9 mm³ for ATO ($P = 0.6723$, 2-tailed Student's t test). The mean age at death for the untreated mice was 4.8 ± 0.4 months, whereas it was 7.4 ± 0.7 months for the treated mice. All of the untreated mice were euthanized for reasons of tumor burden. Of the ATO-treated mice, 1 was euthanized for non-tumor-related health issues, and 5 survived more than 9.5 months (1 died due to tumor; the remaining 4 were euthanized to terminate the study). These animals did not show tumor in follow-up MRI, and there was no tumor in histopathological analysis of their cerebellum (Figure 7A). Histopathological analysis of liver, kidney, heart, lung, and spleen samples from ATO-treated animals did not show any organ toxicity.

When they were available, the tumors from mice treated with ATO were compared with tumors from untreated animals by histology and IHC for TUNEL. H&E sections in both groups showed a malignant small blue cell tumor with occasional pseudorosettes, numerous mitoses, and apoptotic bodies (Figure 7C). There were

no significant differences in the morphology of the tumors, number of mitoses, degree of necrosis, and proliferative index. The number of apoptotic bodies and cells stained in the TUNEL assay appeared more abundant in the treated group, but no statistically significant differences were observed. This lack of difference in morphological analysis was most likely due to bias in availability of the tumor samples for pathological studies. In the ATO group, animals with big tumors that died early in the study were used for histopathological evaluation. However, best responders that survived the longest did not have tumor available for comparison.

We also analyzed molecular response to ATO treatment in a group of ND2:SmoA1 animals. We extracted RNA from frozen tissue samples from normal cerebellum of WT C57BL/6 mice, tumors from control mice, and tumors from ATO-treated mice. We compared expression of GLI target gene expression of *PTCH1* and *N-myc* (Figure 7D). Control tumors had higher expression of GLI target genes compared with the normal cerebellum, as expected due to activated Hh pathway. ATO treated mice had a statistically significant decrease in GLI target gene expression.

Discussion

Starting in the 17th century, arsenic was the primary therapy for treating leukemia, specifically chronic myelogenous leukemia (CML). Its use declined upon the introduction of radiotherapy and chemotherapy (43). Arsenic, in the form of ATO, is now a component of APL therapy. We believe our present work to be novel in its demonstration of ATO as an inhibitor of Hh/GLI signaling. Given the challenges with resistance to Smoothed inhibitors, agents that target GLI have a direct rationale.

We present data indicating that ATO inhibits GLI1 activity, but does not induce degradation of the GLI1 protein (Figures 1–3 and 6). Earlier work has shown that ATO is cytotoxic in ESFT cells at similar concentrations. Jung et al. showed that ATO induced apoptosis via an increase in the phosphorylation status of JNK, but did not pro-

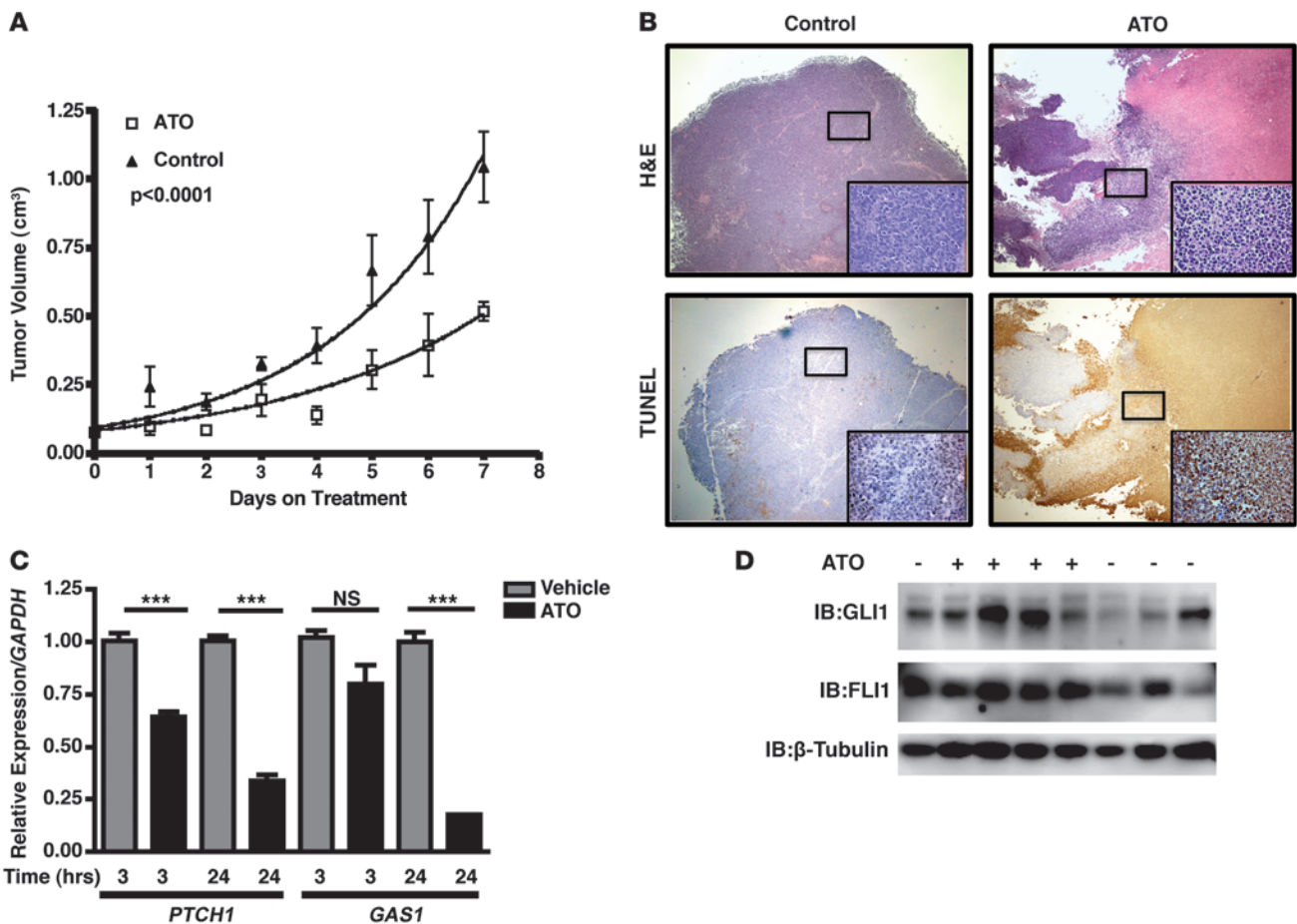


Figure 6

ATO inhibits ESFT cell proliferation in vivo in a mouse xenograft model. (A) TC-71 ESFT cells were implanted intramuscularly to SCID mice. When xenografts became palpable, animals were treated with i.p. injections of PBS control ($n = 8$) or 0.15 mg/kg ATO ($n = 8$) every other day until their tumors reached 1 cm³ ($P < 0.0001$, curve regression and F test). (B) Tumors from the mice in A were analyzed by H&E and IHC for TUNEL as a marker of apoptosis. Boxed regions show viable cells presented at higher magnification in the insets. Main panel images are at $\times 40$ and the insets are at $\times 400$ magnification. (C) Mice with TC-71 xenografts were euthanized at 3 and 24 hours after i.p. injection of PBS or 0.15 mg/kg ATO. qRT-PCR was performed in order to quantify changes in GLI target genes *PTCH1* and *GAS1* of control versus ATO-treated tumors. Expression was normalized to *GAPDH* levels. Mean \pm SD relative expression levels were calculated using the comparative Ct method. *** $P < 0.0001$, 2-tailed Student's t test. Each condition was performed in triplicate. (D) Protein was extracted from frozen tumor samples (4 ATO treated, 4 control) and was subject to SDS-PAGE followed by IB with anti-GLI1, anti-FLI1, and anti- β -tubulin antibodies.

pose a molecular mechanism to explain it (44). We provide evidence that inhibiting JNK activity has no effect on ESFT cell viability with or without ATO, which indicates that JNK activation is not required for ATO's cytotoxicity in ESFT cells. Mathieu et al. provided evidence that ATO causes apoptosis of ESFT and proposed that ATO inhibition of NF- κ B was the possible mechanism (45). However, NF- κ B knockdown in ESFT cells has no effect on viability under normal growth conditions (46). In our experience, ATO did not inhibit NF- κ B in the ESFT cell line TC-71, and activation of NF- κ B did not alter cell viability in the presence or absence of ATO. Therefore, it is unlikely that inhibition of NF- κ B by ATO is the molecular mechanism for ATO-mediated ESFT cytotoxicity in our studies.

We previously demonstrated that GLI1 is a direct transcriptional target of EWS-FLI1 and that it is activated by a noncanonical mechanism irrespective of Hh ligand and Smoothened. Furthermore, proper GLI1 activity is required to maintain malignant phenotype of ESFT cells (15–17). We propose that ATO is cytotoxic in ESFT

cells, at least in part through the inhibition of GLI1. ATO does not alter intracellular localization of GLI1 protein nor binding of GLI1 to DNA. Our data indicate that ATO directly binds to GLI1. In APL, ATO's proposed mechanism of action is degradation of the PML-RAR fusion protein (18). In acute myelogenous leukemia (AML), arsenic has been shown to degrade another fusion protein, AML1/MDS1/EVI1 (47). Arsenic has previously been shown to bind to cysteine residues (21, 23, 48). A recent paper established that arsenic causes degradation of PML-RAR by directing binding to cysteine residue in the zinc finger domain of the PML portion of the fusion protein (49). The authors showed that this interaction occurs in the nucleus and results in a conformational change that allows increased sumoylation and subsequent ubiquitination, leading to degradation. GLI1 is a cysteine-rich protein and has 5 zinc finger binding domains that contain cysteine residues. Given the evidence that arsenic directly binds to GLI1, it is highly plausible that ATO also binds to the zinc finger domains in GLI1, as it does to PML. How

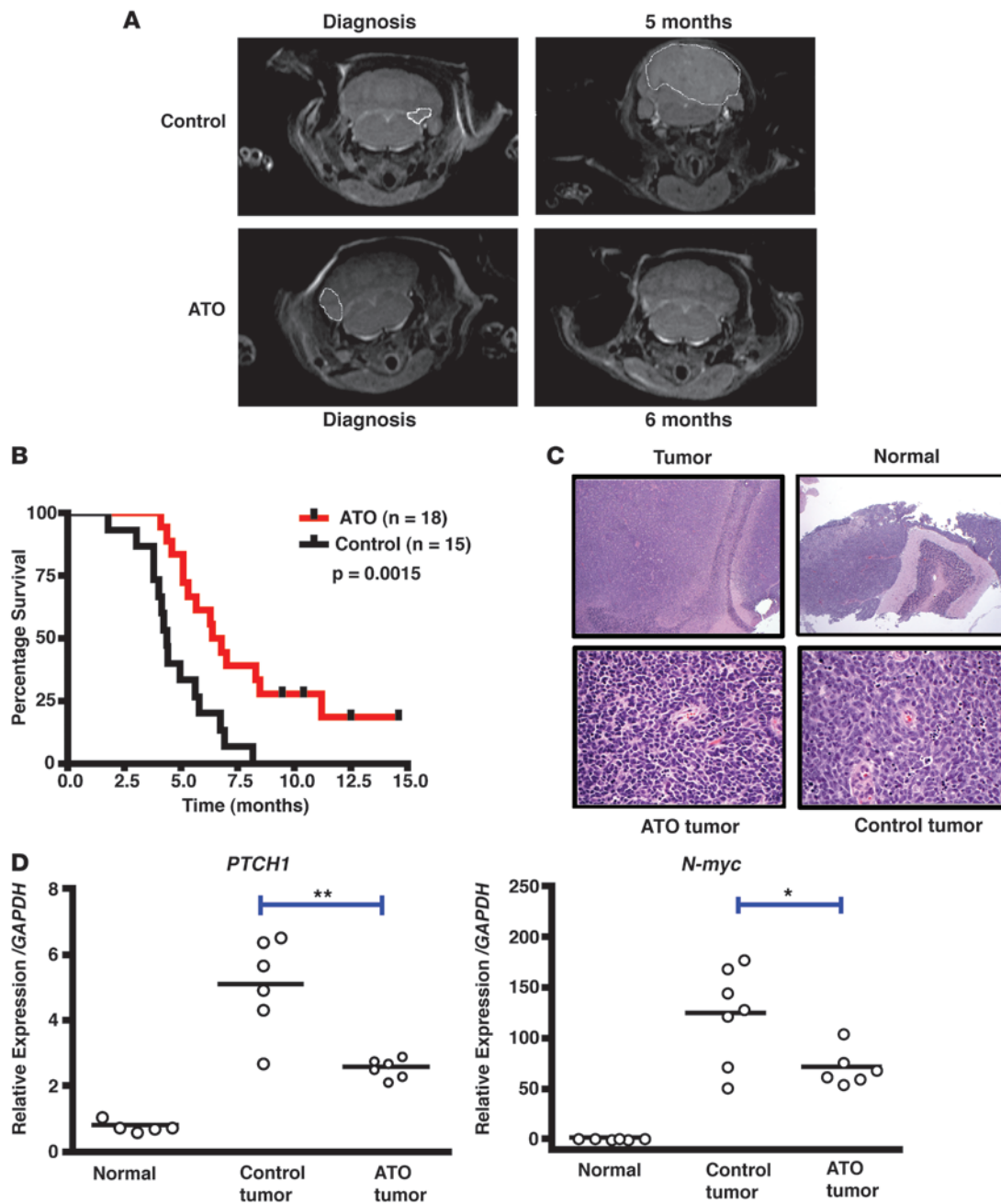


Figure 7

Survival of ND2:SMO1 mice is increased by ATO treatment. **(A)** MRI images of representative animals before treatment and 5–6 months after treatment. Dashed circles denote tumors. **(B)** The survival of ATO-treated ($n = 18$; 0.15 mg/kg 3 times per week) and untreated ($n = 15$) ND2:SMO1 mice were compared ($P = 0.0015$, Kaplan-Meier analysis). Tick marks on the graph represent animals that were still alive at the end of the study. **(C)** Representative H&E sections from control and ATO-treated tumors. In each case, a histologically classical medulloblastoma was observed arising in cerebellum. Low-power images (top) show tumor and normal cerebellum, high-power images (bottom) show tumor. Upper panels images are at $\times 40$ and the lower panel images are at $\times 400$ magnification. **(D)** qRT-PCR was performed to evaluate changes in GLI target genes *PTCH1* and *N-myc* of control tumors ($n = 7$), ATO-treated tumors ($n = 6$), and normal cerebellum ($n = 6$). Expression was normalized to *GAPDH* levels. Mean relative expression levels were calculated using the comparative Ct method. $*P < 0.05$, $**P < 0.01$, 2-tailed Student's *t* test. Each condition was performed in triplicate.

this direct binding inhibits GLI is still unknown and necessitates further investigation. The effect could occur in the nucleus by preventing protein-protein interactions of transcriptional coactivators that bind to GLI1. While the present article was under review, a

paper on ATO and GLI2 was published which has parallels to our findings, but also contains significant differences (37). Their results suggested that ATO inhibits Hh signaling at the level of GLI2. However, the proposed mechanism of action involves reduced protein



stability and altered cilia localization. Since we observed inhibition of GLI1 function shortly after exposure, prior to any protein degradation, our data do not corroborate GLI1 protein stability findings. Furthermore, ATO was able to inhibit GLI1 function independent of primary cilia (Figure 3), even with GLI1 trapped in nucleus (Figure 2). Therefore, preventing GLI1 localization to cilia is again unlikely to be the primary mechanism of action. One has to acknowledge the differences in selected cell lines, experimental methods, and functional differences between GLI1 and GLI2. Even though there were some apparent paradoxical observations related to mechanisms of action, both studies concluded that ATO inhibits Hh signaling at the level of GLI transcription factors.

Previous studies have demonstrated that ATO is cytotoxic in multiple leukemia types. In CML, the presence of the fusion protein BCR-ABL appeared to correlate with ATO sensitivity (50). In addition, the combination of imatinib and arsenic was better than either agent alone in a mouse model of CML (51). A recent publication indicates that expansion of the BCR-ABL leukemic stem cells was dependent on Hh signaling and that the Hh pathway is a potential drug target for patients who relapse after imatinib treatment (52). Another study suggests that GLI1 regulates the proliferation and differentiation of hematopoietic stem cells and myeloid progenitors independent of Smoothened (53). Inhibition of GLI1 (pharmacologically or by siRNA), but not Smoothened, induced apoptosis in chronic lymphocytic leukemia cells (54). These studies also indicated that using Smoothened inhibitors may not be sufficient to treat leukemia and that GLI inhibitors may be more effective. The toxicity of ATO in CML and other leukemia types may be due to its inhibition of GLI in the leukemia stem cell compartment. The status of Hh/GLI signaling in APL patients has not been clearly established. To our knowledge, there is only 1 report that investigated GLI1 expression in APL patients: Bai et al. described 100% of APL cases expressing GLI1 (55). However, their cohort included only 3 APL cases, and the antibody used for IHC was not validated for that method. Nevertheless, if their findings can be confirmed by more reliable methods and larger sample sizes, it is plausible that ATO's effect on APL cells results from inhibition of both PML-RAR and GLI.

Hh signaling has been shown to play an important role in BCC (1, 3, 5). Anecdotally, a Dutch population study that examined the effects of low doses of arsenic concentrations in drinking water on cancer risk found that arsenic did not increase the risk of multiple cancer types. In fact, increasing concentrations of arsenic in the water correlated with a decreased risk of nonmelanoma skin cancers (56). This reduced risk of nonmelanoma skin cancer (which includes BCC) may be partially due to the effects of arsenic on Hh signaling.

A newly published study showed that arsenic activated Hh signaling in primary lung cells and NIH3T3 cells and attempted to link this discovery to arsenic-induced bladder cancer (57). The authors showed that arsenic activated Hh signaling in these cells by inhibiting the GLI3 repressor. However, in this study, sodium arsenite was used, which is a different compound than ATO. It is possible that sodium arsenite has preferential binding to GLI3 over GLI1 and GLI2, and thus activates signaling instead of repressing it. The difference in activation versus repression could also be specific to cell type or species, given that the majority of the study used mouse cells instead of human cells.

A recent phase I trial of a Hh pathway inhibitor that targets Smoothened, GDC-0449, showed promising results in BCC (58). Thus, ATO potentially could be a new therapy for BCC. The Hh

pathway inhibitor GDC-0449 used in the BCC trial was also administered to 1 medulloblastoma patient with metastatic disease who was refractory to multiple treatments. The patient first showed regression of tumor after 2 months of treatment, but eventually relapsed (59). The cause of the relapse was discovered to be a mutation in Smoothened in the patient's tumor that prevented binding of the drug to Smoothened. The same resistance to the drug was also recapitulated in a medulloblastoma mouse model (32). Since we propose that ATO is a GLI inhibitor and inhibits the pathway downstream of Smoothened, it may thus be an effective therapy in medulloblastoma patients that develop resistance to Smoothened inhibitors.

In summary, our results provide strong evidence that ATO inhibits GLI1 protein function in the nucleus. ATO-mediated inhibition of GLI1 was independent of upstream Hh signaling. ATO exhibited marked cytotoxicity on ESFT and medulloblastoma cell lines in vitro and showed promising effects in vivo on ESFT xenografts and a transgenic medulloblastoma mouse model. The pharmacokinetics from a published pediatric phase 1 trial indicate that the peak ATO levels at the maximum tolerated dose are in the 0.5- μ M range, with prolonged exposure tolerated to levels of about 0.1 μ M (60). Our data support continued preclinical evaluation of ATO in tumors that have either upstream pathway activation or transcriptional activation of GLI1. The combination of significant clinical experience with ATO and these mechanistic insights, which we believe to be novel, should lead to extended clinical applications of ATO.

Methods

Cell lines and reagents. COS7, PANC1, and SKNAS cells were grown in DMEM with 10% FBS. All ESFT cell lines, DAOY, D556, and H1299 were grown in RPMI with 10% FBS and 1% HEPES, with the exception of SKES and A673. SKES cells were grown in McCoy's 5a medium with 15% FBS. A673 cells were grown in DMEM supplemented with 1% sodium pyruvate and 10% FBS. CAPAN cells were grown in Iscove DMEM (IMDM) with 1% sodium pyruvate and 20% FBS. CHLA-20 and CHLA-15 cells were grown in IMDM with 1% insulin-transferrin-sodium selenate and 20% FBS. HepG2 cells were grown in DMEM with 10% FBS and 1% nonessential amino acids. KIF3a WT and knockout MEFS were grown in DMEM plus 1% nonessential amino acids, 1% L-glutamine, 1% sodium pyruvate, and G418 (mg/ml). Pharmaceutical-grade ATO was purchased at a concentration of 1 mg/ml in a sterile, nonpyrogenic, clear solution in water using sodium hydroxide and dilute hydrochloric acid to adjust to pH 8 (Cephalon Inc.). The JNK inhibitor SP600125 was purchased from Calbiochem. LPS (Sigma-Aldrich) was used to activate NF- κ B.

Luciferase assays. GLI1 activity was assessed using a pGL3-basic luciferase construct containing 8 \times GLI1-binding sites attached to a chicken lens crystalline promoter (pGL38xGLI; ATCC-Johns Hopkins Special Collections, deposited by P.A. Beachy) and a *Renilla*-TK mutant construct (provided by S. Byers, Georgetown University, Washington, DC, USA). To measure the effects of ATO on GLI1, HepG2 cells were cotransfected with either EGFP-hGLI1 (provided by J. Reiter, UCSF, San Francisco, California, USA) or empty vector control (pEGFP-C1; Clontech) in addition to pGL38xGLI luciferase and *Renilla* constructs with Fugene6 (Roche) according to the manufacturer's protocol. To measure the effects of ATO on other transcription factors, HEPG2 cells were cotransfected with EWS-FLI1 and the EWS-FLI1-responsive luciferase constructs NROB1 (provided by S. Lessnick, University of Utah, Salt Lake City, Utah, USA) or Notch1 (provided by R. Schlegel, Georgetown University, Washington, DC, USA) and the Notch-responsive promoter constructor HES-1 (provided by A. Israel, Institut Pasteur, Paris, France) and empty vector control construct (CIneo or pFlagCMV2) in addition to the *Renilla* construct. To measure the effects of GLI2, COS7 cells were transfected with or without pcDNA4T/O-GLI2 (provided by F. Abergler, University of



Salzberg, Salzberg, Austria) in addition to pGL38xGLI luciferase and *Renilla* constructs with Fugene6. To measure the effects of ATO on GLI1 activity in the nucleus, we transfected COS7 cells with EGFP-GLI1WT, EGFP-GLI1AHA (provided by D. Wu, Yale University, New Haven, Connecticut, USA), and EGFP-GLI1WT cotransfected with HA-tagged DRYK1 (provided by D. Wu) in addition to the pGL38xGLI1 luciferase and *Renilla* constructs. Localization was determined by green fluorescence for GFP-tagged proteins and Hoechst dye for the nucleus on a Nikon Eclipse *Ti* microscope using a $\times 40$ lens. In studies using drug treatment, cells were treated with drug 24 hours after transfection, and then luciferase activity was measured 24 hours after treatment. Luciferase assays in the KIF3a WT and knockout cells were done similar to those described above; however, the MEFs were transfected using electroporation in OptiMEM medium (Invitrogen) using a Cell-Porator (Invitrogen) at 350 V. To measure the effect of JNK inhibition in combination with ATO treatment on GLI1 activity, COS7 cells were transfected with EGFP-hGLI1 in addition to pGL38xGLI luciferase and *Renilla* constructs with Fugene6 (Roche) according to the manufacturer's protocol. 24 hours after transfection, cells were drug treated; luciferase activity was measured 24 hours after treatment. All luciferase assays were performed using a dual luciferase assay kit according to the manufacturer's protocol (Promega).

Immunofluorescence for visualization of primary cilia. KIF3a WT or knockout cells were plated on circular coverslips in 12-well plates and grown to confluency. Cells were then serum starved for 24 hours to form primary cilia, treated with ATO for another 24 hours in the absence of serum, and then fixed in 4% paraformaldehyde for 20 minutes. Cells were permeabilized with PBS with 0.5% Triton X-100 for 5 minutes, and nonspecific binding sites were blocked with 2% BSA in PBST (PBS with 0.5% Tween-20). Cells were stained with primary antibody for acetylated tubulin (Sigma-Aldrich, 1:5,000) diluted in 2% BSA in PBST overnight at 4°C. After washing 3 times in PBST, cells were incubated for 1 hour with Alexa Fluor 488-conjugated secondary antibodies (Invitrogen) in 2% BSA in PBST. Cilia formation was then viewed using an Olympus Fluoview-FV300 Laser Scanning Confocal System.

Cloning and protein expression of recombinant full-length GLI1. GLI1 cDNA was isolated from the EGFP-hGLI1 using PCR with the following primers: forward, 5'-TTCAACTCGATGACCCACC-3'; reverse, 5'-GGCAGTAGAGTTGAGGAATT-3'. The forward primer added an ATG start site, and the reverse removed the stop codon. The PCR product was then TA cloned into the pCRII vector (Invitrogen) according to the manufacturer's instructions. The N-terminal HIS and T7 tags were removed from pET28B+ (Novagen; EMD Biosciences Inc.) by restriction digest with NcoI and BamHI followed by mungbean endonuclease treatment to make blunt ends. The blunt ends were ligated together using T4 DNA ligase (Roche) according to the manufacturer's instructions. In order to have the C-terminal HIS tag in frame with the GLI1 sequence, both the modified pET28B+ and GLI1 in TA vector pCRII were first cut with NotI, and then the overhang was filled in with DNA polymerase I-klenow fragment (New England Biolabs) according to the manufacturer's protocol to make a blunt end. Both were cut with SacI, and the GLI1 sequence was ligated to the pET28B+ using T4 DNA ligase. The resulting vector pET28B+/GLI1 was verified by sequencing. BL21-CodonPlus (DE3)-RIPL-competent cells (Stratagene) containing the expression vector were grown overnight at 37°C in Luria-Bertani media with 50 µg/ml kanamycin and chloramphenicol. The culture was then diluted 1:20 in 1 l fresh Luria-Bertani media without antibiotics and allowed to grow at 37°C until an optical density of 0.6 was observed at 600 nm. Protein production was initiated by adding 1 mM isopropyl-D-1-thiogalactopyranoside, and bacteria were cultured for an additional 4 hours at 37°C. The majority of the protein was found to be in the insoluble inclusion body fraction of the bacteria. The insoluble and soluble fractions were separated and isolated from the whole bacteria prep with BugBuster protein extraction reagent (Novagen) according to the manufacturer's protocol.

Recombinant GLI1 protein preparation. An inclusion body pellet corresponding to 1 l bacterial culture was resuspended in 50 ml of buffer containing 20 mM Tris-HCL (pH 7.5), 500 mM NaCl, 5 mM imidazole, and 6 M guanidine HCL. The supernatant was filtered (0.22 µm pore size) and applied to a 1-ml prepacked Hitrap metal chelating column on an AKTA-Explorer chromatography system kept at 4°C (GE Healthcare). Initially, metal chelating columns were washed with 10 ml H₂O; charged with 10 ml of 100 mM NiSO₄; washed again with H₂O; and equilibrated with 20 mM Tris-HCL (pH 7.5), 500 mM NaCl, 5 mM imidazole, and 6 M guanidine HCL. The sample was loaded on the column, and buffer was changed to 10 ml of 20 mM Tris-HCL (pH 7.5), 500 mM NaCl, 5 mM imidazole, and 6 M urea in a gradient. The protein was then refolded on the column using a slow 30-ml linear gradient that changed to 20 mM Tris-HCL (pH 7.5), 500 mM NaCl, 5 mM imidazole, and 1 mM ZnCl₂. Protein was eluted from the column by a slow 20-ml linear gradient from 5 mM to 2 M imidazole. ZnCl₂ was added to refolding and elution buffers to help maintain the integrity of the zinc finger DNA binding domains. Aliquots (1 ml) were collected and then applied to a 6% acrylamide gel for Coomassie staining (ThermoScientific).

SPR studies for direct DNA binding. SPR studies were performed on a Biacore T-100 instrument at room temperature. GLI1 protein was captured on the second flow cell of a CM5 sensorchip by amine coupling method in pH 5.0 glycine buffer (~8,000 RU). The first flow cell was left empty for background signal subtraction. All DNA oligonucleotides were diluted in the running buffer (10 mM HEPES, pH 7.4; 90 mM KCl₂; 1 mM ZnCl₂; 0.5 mM EDTA; and 0.05% p-20). Kinetics analysis was done by injecting WT (forward, 5'-AGTACTCTGGGTGGTCTCT-3'; reverse, 5'-AGAGACCACCCAGGTAGCT-3') and mutant (forward, 5'-AGTACTCTCCCACTTCTCT-3'; reverse, 5'-AGAGAAGTGGGAGGTAGT-3') oligonucleotides over GLI1 captured and control surfaces. Each injection was done with 60 seconds association time and 360 seconds dissociation time. For surface regeneration, a 30-second pulse of 1 M NaCl was used. Each concentration was repeated 3 times, and the results were analyzed using Biacore T-100 evaluation software. Experiments were repeated at least 3 times. For reciprocal experiments, the same GLI binding site oligos were synthesized with a Biotin molecule on the 5' end of 1 strand and captured on a streptavidin-coated chip.

In vitro FAsH-binding assays. In vitro FAsH-EDT₂-binding assays (Invitrogen) were done similar to previously published methods (21, 35). Briefly, 40 nM recombinant full-length GLI1 was preincubated with 200, 100, 50, and 25 µM ATO for 2 hours in 1× PBS. After 2 hours, 200 nM FAsH compound was added and incubated for 20 minutes. Recombinant EWS-FLI1 with FAsH alone was used as a negative control. 50 µM BAL (Invitrogen) was used as a positive control, as it quenches FAsH by directly binding to it. Fluorescence signal was measured with excitation at 508 nm and emission at 528 nm in a PerkinElmer EnVision Multilabel Plate Reader.

ReAsH-EDT₂ labeling in cells. COS7 cells expressing EGFP-fused constructs were grown on cover glasses and labeled with 2.5 µM ReAsH-EDT₂ for 1 hour at 37°C in serum-free Opti-MEM (Invitrogen). After thoroughly washing with 250 µM BAL buffer, cells were then live imaged using an Olympus Fluoview-FV300 Laser Scanning Confocal System.

Cell fractionation. Cells were rinsed 3 times with cold 1× PBS, subsequently lysed in cold hypotonic lysis buffer (10 mM Tris-HCL, pH 7.5, and 0.2 mM magnesium chloride), collected, and homogenized with 35 strokes of a glass dounce homogenizer. Homogenates were centrifuged for 10 minutes at 3,000 g, and the supernatant was transferred to an ultracentrifuge tube containing a 1.25 M sucrose pad and protease inhibitors (250 mM sodium fluoride, 5 mM sodium orthovanadate, 5× mini complete protease cocktail [Roche], and 5 mM EDTA). This preparation was centrifuged for 1 hour at 150,000 g (Beckman L8-M ultracentrifuge); protein from the resulting supernatant was precipitated with 100% ethanol and centrifuged again for 1 hour at 150,000 g; and the resulting pellet, designated as the cytoplasmic



pool, was resuspended in SDS sample buffer (2% SDS; 60 mM Tris-HCl, pH 6.8; and 10% glycerol). The pellet from the original centrifugation (nuclei and membrane) was rinsed in hypotonic lysis buffer, recentrifuged, and dried briefly at 4°C. This pellet was resuspended in NP-40 buffer with protease inhibitors (1% NP-40; 150 mM sodium chloride; and 50 mM Tris-HCl, pH 8.0; with 1 mM sodium orthovanadate, 50 mM sodium fluoride, and 1× mini complete protease inhibitor cocktail), briefly vortexed, and allowed to solubilize at 4°C with gentle agitation. The suspension was collected by centrifugation at 3,000 g, resulting in a supernatant (membrane pool) and a pellet (nuclear pool). The pellet was rinsed once in fresh NP-40 buffer and subsequently resuspended in SDS sample buffer.

IB. Whole cell lysates from cells grown to near confluency or tumor samples were subject to SDS-PAGE and then transferred to an Immobilon-P membrane (Millipore). Membranes were then subjected to blocking in 5% nonfat dry milk in 1× TTBS (20 mM Tris-HCL, pH 7.5; 150 mM NaCl; and 0.5% Tween 20) for 1 hour. Dilutions for primary antibodies were as follows: anti-GLI1 (L42B10) for human GLI1 at 1:1,000 (Cell Signaling), anti-GLI1 (V812) for endogenous Cos7 GLI1 at 1:1,000 (Cell Signaling), anti-GLI2 at 1:1,000 (Cell Signaling), anti-FLI1 at 1:2,000 (Santa Cruz Biotechnology), anti-Notch at 1:1,000 (Cell Signaling), anti-actin-HRP (C-11) at 1:3,000 (Santa Cruz Biotechnology), anti-β-tubulin at 1:5,000 (MP Biomedicals), anti-KIF3a at 1:5,000 (Sigma-Aldrich), anti-lamin A/C at 1:2,000 (Cell Signaling), phospho-JNK at 1:1,000 (Cell Signaling), JNK at 1:1,000 (Cell Signaling), phospho-NF-κB p65 at 1:1,000 (Cell Signaling), and NF-κB p65 at 1:1,000 (Cell Signaling). Primary antibodies were added to the membrane in 5% nonfat dry milk in 1× TTBS for 1 hour. The membrane was then washed 3 times in 1× TTBS and HRP-linked anti-rabbit or anti-mouse secondary antibody (GE Healthcare) was added for 1 hour. Blots were washed 3 times in 1× TTBS and then developed using Millipore Immobilon Western Chemiluminescent HRP Substrate per the manufacturer's instructions (Millipore Corp.). Chemiluminescence was detected using a Fujifilm LAS-3000 imaging system. Densitometry values were obtained using Multigauge software.

qRT-PCR. For in vitro studies, cells were treated with or without ATO for 12 hours. For in vivo studies, frozen tumors samples were homogenized in liquid nitrogen using a mortar and pestle. Total RNA was extracted by TRIzol (Invitrogen) and reverse transcribed using the Transcriptor First Strand cDNA Synthesis Kit (Roche) according to the manufacturer's protocol. PCR was performed using an Eppendorf Mastercycler realplex using Taqman Gene Expression Master Mix according to the manufacturer's instructions with Taqman Gene expression primers for *GLI1*, *PTCH1*, *GAS1*, *N-myc*, and *GAPDH* (Applied Biosystems). Data were analyzed for expression relative to *GAPDH* using the comparative Ct method. Each experiment was performed in triplicate.

IHC. To determine necrosis, slides were stained with hematoxylin (Harris Modified Hematoxylin; Fisher) at a 1:17 dilution for 2 minutes at room temperature, blue in 1% ammonium hydroxide for 1 minute at room temperature, dehydrated, and mounted with Acrymount. TUNEL assay was performed using the Apotag kit from Millipore. Briefly, 5-μm sections from formalin-fixed, paraffin-embedded tissues were deparaffinized with xylenes and rehydrated through a graded alcohol series. Heat-induced epitope retrieval was performed by immersing the tissue sections at 98°C for 20 minutes in 10 mM citrate buffer (pH 6.0) with 0.05% Tween. Slides were pretreated with 3% hydrogen peroxide at room temperature, 10 mM sodium citrate at 65°C, and equilibration buffer. Slides were exposed to terminal transferase and digoxigenin-labeled dUTP in reaction buffer for 2 hours at 37°C, stopped in wash buffer, and blocked with 10% normal goat serum. Slides were exposed to HRP-conjugated anti-digoxigenin secondary antibodies (Roche) and DAB chromagen (Dako). Quantification of necrosis and TUNEL staining was performed by a pathologist in a blinded fashion with coded samples.

Cellular proliferation assays. Cellular proliferation was assessed by triplicate plating at a density of 5,000–10,000 cells/well, depending on the cell line, in a 96-well plate. ATO at varying concentrations or vehicle alone (10 μM H₂O) were added to cells in standard growth media for that cell line the following morning after plating, once the cells had attached. Fresh media containing drug or vehicle was added every 2–3 days. Viable cells were quantified using 10 μl WST-1 Reagent (Roche) according to the manufacturer's protocol after 4 days. IC₅₀ values were calculated by sigmoidal dose-response curve fit using Prism Graphpad 4.0 for Macintosh. For Supplemental Figures 7–9, cellular proliferation was assessed using a real-time Electric Cell-substrate Impedance Sensing assay (RTCA DP Analyzer; Roche), and measurements were taken every 10 minutes for 24 hours. Cell Index (CI) is derived as a change in measured electrical impedance to represent cell status. When more cells are attached on the electrodes, the CI values are larger. Thus, CI is a quantitative measure of cell number present in a well. A change in cell status, such as cell morphology, cell adhesion, or cell viability, will lead to a change in CI.

Animal studies. 1 × 10⁶ TC-71 cells in 100 μl of HBSS were orthotopically injected into the gastrocnemius muscle of 4-week-old SCID-beige mice (Charles River). We randomized mice to treatment groups receiving every other day i.p. injections of vehicle (PBS) or ATO at a dose of 0.15 mg/kg in 100 μl when tumors were palpable. We measured tumor length and width every 1–2 days and calculated volume with the formula ($D \times d^2$) × π/6, where *D* is the longest diameter and *d* is the shorter diameter. ND2:SmOA1 homozygous mice were as previously described (42). Tumor was detected by monitoring for the presence of clinical signs of disease, such as decreased motor and coordination functions, a deformed cranium and megalencephaly, a hunched back, and weight loss. MRI was subsequently performed to confirm the presence of a defined medulloblastoma (MB) tumor in the cerebellum as well as to identify localization and assess volume. Once animals had a detectable tumor, they began treatment with ATO at a dose of 0.15 mg/kg 3 times per week. The end point of the study was when animals were euthanized due to lack of movement around the cage, which resulted in an inability to reach food and water, or weight loss greater than 15% of the total body weight. Animals chosen for Kaplan-Meier analysis between ATO treatment and control were matched based on age of tumor onset as well as tumor size at the start of treatment. All animal studies were approved by the Georgetown University Institutional Animal Care and Use Committee.

Statistics. All statistical analysis tests were performed using Prism Graphpad 4.0 for Macintosh. Survival curves were analyzed by the Kaplan-Meier method. Correlation was assessed using nonparametric Spearman test. Significance of differences with regard to tumor size was determined by curve regression and *F* test. IC₅₀ values were calculating using a nonlinear sigmoidal dose-response curve fit. Other determinations of significance were assessed by 2-tailed Student's *t* test, as indicated. A *P* value less than 0.05 was considered significant.

Acknowledgments

We thank Jeremy Reiter for the EGFP-hGLI1 construct and KIF3a WT and knockout cells, Fritz Aberger for the GLI2 construct, James Olson for the ND2:SMOA1 medulloblastoma mouse model, Richard Schlegel for the Notch1 construct, Stephen Lessnick for the NROB1 construct, Alain Israel for the Hes1 construct, Dianqing Wu for the GLI1AHA and Dyrk1 constructs, and Stephen Byers for the modified *Renilla* construct. We greatly appreciated helpful discussions with Bill Matsui and Phil Beachy. We also thank Georgetown University and the Lombardi Comprehensive Cancer Center's Preclinical Imaging Research Laboratory for MRI; Histopathology and Tissue Shared Resource for H&E, TUNEL, and IHC; Microscopy and Imaging Shared Resource for technical help with confocal microscopy; and Biacore Molecular Interactions Shared



Resource for SPR experiments. These studies were supported by grants from Cancer Center Support Grant P30 CA051008 for use of Shared Resources, the Children's Cancer Foundation of Baltimore, Maryland (to A. Üren), and Accelerate Brain Cancer Cure, Washington, DC (to T.J. Macdonald and C. Albanese) as well as by NIH grant CA88004 (to J.A. Toretsky).

Received for publication March 4, 2010, and accepted in revised form October 13, 2010.

Address correspondence to: Aykut Üren, 3970 Reservoir Rd. NW, NRB, Room E312, Washington, DC 20057, USA. Phone: 202.687.9504; Fax: 202.687.1434; E-mail: au26@georgetown.edu.

1. Hahn H, et al. Mutations of the human homolog of Drosophila patched in the nevoid basal cell carcinoma syndrome. *Cell*. 1996;85(6):841–851.
2. Pietsch T, et al. Medulloblastomas of the desmoplastic variant carry mutations of the human homologue of Drosophila patched. *Cancer Res*. 1997;57(11):2085–2088.
3. Reifenberger J, et al. Missense mutations in SMOH in sporadic basal cell carcinomas of the skin and primitive neuroectodermal tumors of the central nervous system. *Cancer Res*. 1998;58(9):1798–1803.
4. Berman DM, et al. Medulloblastoma growth inhibition by hedgehog pathway blockade. *Science*. 2002;297(5586):1559–1561.
5. Regl G, et al. Human GLI2 and GLI1 are part of a positive feedback mechanism in Basal Cell Carcinoma. *Oncogene*. 2002;21(36):5529–5539.
6. Taylor MD, et al. Mutations in SUFU predispose to medulloblastoma. *Nat Genet*. 2002;31(3):306–310.
7. Di Marcotullio L, et al. REN(KCTD11) is a suppressor of Hedgehog signaling and is deleted in human medulloblastoma. *Proc Natl Acad Sci U S A*. 2004;101(29):10833–10838.
8. Kimura H, Stephen D, Joyner A, Curran T. Gli1 is important for medulloblastoma formation in Ptc1^{-/-} mice. *Oncogene*. 2005;24(25):4026–4036.
9. Pritchard JJ, Olson JM. Methylation of PTCH1, the Patched-1 gene, in a panel of primary medulloblastomas. *Cancer Genet Cytogenet*. 2008;180(1):47–50.
10. Kinzler KW, et al. Identification of an amplified, highly expressed gene in a human glioma. *Science*. 1987;236(4797):70–73.
11. Nesslering M, et al. Candidate genes in breast cancer revealed by microarray-based comparative genomic hybridization of archived tissue. *Cancer Res*. 2005;65(2):439–447.
12. Roberts WM, Douglass EC, Peiper SC, Houghton PJ, Look AT. Amplification of the gli gene in childhood sarcomas. *Cancer Res*. 1989;49(19):5407–5413.
13. Dahlen A, et al. Activation of the GLI oncogene through fusion with the beta-actin gene (ACTB) in a group of distinctive pericytic neoplasms: pericytoma with (7;12). *Am J Pathol*. 2004;164(5):1645–1653.
14. Bhatia N, et al. Gli2 is targeted for ubiquitination and degradation by beta-TrCP ubiquitin ligase. *J Biol Chem*. 2006;281(28):19320–19326.
15. Beauchamp E, et al. GLI1 Is a Direct Transcriptional Target of EWS-FLI1 Oncoprotein. *J Biol Chem*. 2009;284(14):9074.
16. Joo J, et al. GLI1 is a central mediator of EWS/FLI1 signaling in Ewing tumors. *PLoS One*. 2009;4(10):e7608.
17. Zwerner JP, et al. The EWS/FLI1 oncogenic transcription factor deregulates GLI1. *Oncogene*. 2008;27(23):3282–3291.
18. Nasr R, et al. Eradication of acute promyelocytic leukemia-initiating cells through PML-RARA degradation. *Nat Med*. 2008;14(12):1333–1342.
19. Cavigelli M, Li WW, Lin A, Su B, Yoshioka K, Karin M. The tumor promoter arsenite stimulates AP-1 activity by inhibiting a JNK phosphatase. *EMBO J*. 1996;15(22):6269–6279.
20. Hayashi T, et al. Arsenic trioxide inhibits growth of human multiple myeloma cells in the bone marrow microenvironment. *Mol Cancer Ther*. 2002;1(10):851–860.
21. Kapahi P, et al. Inhibition of NF-kappa B activation by arsenite through reaction with a critical cysteine in the activation loop of I kappa B kinase. *J Biol Chem*. 2000;275(46):36062–36066.
22. Mann KK, et al. Antimony trioxide-induced apoptosis is dependent on SEK1/JNK signaling. *Toxicol Lett*. 2006;160(2):158–170.
23. Lu J, Chew EH, Holmgren A. Targeting thioredoxin reductase is a basis for cancer therapy by arsenic trioxide. *Proc Natl Acad Sci U S A*. 2007;104(30):12288–12293.
24. Mao J, et al. Regulation of Gli1 transcriptional activity in the nucleus by Dyrk1. *J Biol Chem*. 2002;277(38):35156–35161.
25. Corbit KC, Aanstad P, Singla V, Norman AR, Stainier DY, Reiter JF. Vertebrate Smoothed functions at the primary cilium. *Nature*. 2005;437(7061):1018–1021.
26. Han YG, et al. Hedgehog signaling and primary cilia are required for the formation of adult neural stem cells. *Nat Neurosci*. 2008;11(3):277–284.
27. Huangfu D, Liu A, Rakeam AS, Murcia NS, Niswander L, Anderson KV. Hedgehog signalling in the mouse requires intraflagellar transport proteins. *Nature*. 2003;426(6962):83–87.
28. Liu A, Wang B, Niswander LA. Mouse intraflagellar transport proteins regulate both the activator and repressor functions of Gli transcription factors. *Development*. 2005;132(13):3103–3111.
29. May SR, et al. Loss of the retrograde motor for IFT disrupts localization of Smo to cilia and prevents the expression of both activator and repressor functions of Gli. *Dev Biol*. 2005;287(2):378–389.
30. Rohatgi R, Milenkovic L, Scott MP. Patched1 regulates hedgehog signaling at the primary cilium. *Science*. 2007;317(5836):372–376.
31. Spassky N, et al. Primary cilia are required for cerebellar development and Shh-dependent expansion of progenitor pool. *Dev Biol*. 2008;317(1):246–259.
32. Yauch RL, et al. Smoothed mutation confers resistance to a Hedgehog pathway inhibitor in medulloblastoma. *Science*. 2009;326(5952):572–574.
33. Wong SY, et al. Primary cilia can both mediate and suppress Hedgehog pathway-dependent tumorigenesis. *Nat Med*. 2009;15(9):1055–1061.
34. Üren A, Tcherkasskaya O, Toretsky JA. Recombinant EWS-FLI1 oncoprotein activates transcription. *Biochemistry*. 2004;43(42):13579–13589.
35. Griffin BA, Adams SR, Tsien RY. Specific covalent labeling of recombinant protein molecules inside live cells. *Science*. 1998;281(5374):269–272.
36. Agren M, Kogerman P, Kleman MI, Wessling M, Toftgard R. Expression of the PTCH1 tumor suppressor gene is regulated by alternative promoters and a single functional Gli-binding site. *Gene*. 2004;330:101–114.
37. Kim J, Lee JJ, Gardner D, Beachy PA. Arsenic antagonizes the Hedgehog pathway by preventing ciliary accumulation and reducing stability of the Gli2 transcriptional effector. *Proc Natl Acad Sci U S A*. 2010;107(30):13432–13437.
38. Kinjo K, et al. Arsenic trioxide (As2O3)-induced apoptosis and differentiation in retinoic acid-resistant acute promyelocytic leukemia model in hGM-CSF-producing transgenic SCID mice. *Leukemia*. 2000;14(3):431–438.
39. Lallemand-Breitenbach V, et al. Retinoic acid and arsenite synergize to eradicate leukemic cells in a mouse model of acute promyelocytic leukemia. *J Exp Med*. 1999;189(7):1043–1052.
40. Li Y, Sun X, Wang L, Zhou Z, Kang YJ. Myocardial toxicity of arsenic trioxide in a mouse model. *Cardiovasc Toxicol*. 2002;2(1):63–73.
41. Hallahan AR, et al. The SmoA1 mouse model reveals that notch signaling is critical for the growth and survival of sonic hedgehog-induced medulloblastomas. *Cancer Res*. 2004;64(21):7794–7800.
42. Hatton BA, et al. The Smo/Smo model: hedgehog-induced medulloblastoma with 90% incidence and leptomeningeal spread. *Cancer Res*. 2008;68(6):1768–1776.
43. Waxman S, Anderson KC. History of the development of arsenic derivatives in cancer therapy. *Oncologist*. 2001;6 suppl 2:3–10.
44. Jung HS, et al. Arsenic trioxide concentration determines the fate of Ewing's sarcoma family tumors and neuroblastoma cells in vitro. *FEBS Lett*. 2006;580(20):4969–4975.
45. Mathieu J, Besancon F. Clinically tolerable concentrations of arsenic trioxide induce p53-independent cell death and repress NF-kappa B activation in Ewing sarcoma cells. *Int J Cancer*. 2006;119(7):1723–1727.
46. White DE, Burchill SA. BAY 11-7082 induces cell death through NF-kappaB-independent mechanisms in the Ewing's sarcoma family of tumours. *Cancer Lett*. 2008;268(2):212–224.
47. Shackelford D, Kenific C, Bluszstajn A, Waxman S, Ren R. Targeted degradation of the AML1/MDS1/EVI1 oncoprotein by arsenic trioxide. *Cancer Res*. 2006;66(23):11360–11369.
48. Jiang G, Gong Z, Li XF, Cullen WR, Le XC. Interaction of trivalent arsenicals with metallothionein. *Chem Res Toxicol*. 2003;16(7):873–880.
49. Zhang XW, et al. Arsenic trioxide controls the fate of the PML-RARalpha oncoprotein by directly binding PML. *Science*. 2010;328(5975):240–243.
50. Puccetti E, et al. BCR-ABL mediates arsenic trioxide-induced apoptosis independently of its aberrant kinase activity. *Cancer Res*. 2000;60(13):3409–3413.
51. Zhang QY, et al. A systems biology understanding of the synergistic effects of arsenic sulfide and Imatinib in BCR/ABL-associated leukemia. *Proc Natl Acad Sci U S A*. 2009;106(9):3378–3383.
52. Dierks C, et al. Expansion of Bcr-Abl-positive leukemic stem cells is dependent on Hedgehog pathway activation. *Cancer Cell*. 2008;14(3):238–249.
53. Merchant A, Joseph G, Wang Q, Brennan S, Matsui W. Gli1 regulates the proliferation and differentiation of HSC and myeloid progenitors. *Blood*. 2010;115(12):2391–2396.
54. Desch P, et al. Inhibition of GLI, but not Smoothed, induces apoptosis in chronic lymphocytic leukemia cells. *Oncogene*. 2010;29(35):4885–4895.
55. Bai LY, et al. Differential expression of Sonic hedgehog and Gli1 in hematological malignancies. *Leukemia*. 2008;22(1):226–228.
56. Baastrup R, et al. Arsenic in drinking-water and risk for cancer in Denmark. *Environ Health Perspect*. 2008;116(2):231–237.
57. Fei DL, et al. Activation of Hedgehog signaling by the environmental toxicant arsenic may contribute to the etiology of arsenic-induced tumors. *Cancer Res*. 2010;70(5):1981–1988.
58. Von Hoff DD, et al. Inhibition of the hedgehog pathway in advanced basal-cell carcinoma. *N Engl J Med*. 2009;361(12):1164–1172.
59. Rudin CM, et al. Treatment of medulloblastoma with hedgehog pathway inhibitor GDC-0449. *N Engl J Med*. 2009;361(12):1173–1178.
60. Fox E, et al. Phase I trial and pharmacokinetic study of arsenic trioxide in children and adolescents with refractory or relapsed acute leukemia, including acute promyelocytic leukemia or lymphoma. *Blood*. 2008;111(2):566–573.